PHYSICAL REVIEW B VOLUME 27, NUMBER 4 15 FEBRUARY 1983

Study of the K edges of $3d$ transition metals in pure and oxide form by x-ray-absorption spectroscopy

L. A. Grunes*
School of Applied and Engineering Physics and Materials Science Center, Cornell University, Ithaca, New York, 14853
(Received 9 September 1982)

The metal K-edge absorption spectra of $3d$ transition metals and oxides are measured by x-ray-absorption spectroscopy. Experiments are performed on metal foils or fine powders dusted onto Scotch tape, at the Cornell High Energy Synchrotron Source. Comparisons to theory are made for both the metal and oxide data. We concentrate on the spectral near-edge structure (NES) and attempt to interpret its origins. For the metals, we find excellent agreement between the data and one-electron calculations. This agreement is much closer than previously found for the L_{23} edges in the same materials. The picture for the oxide near-edge structure is not so auspicious. Although symmetry-based molecular-orbital (MO) theory has been widely invoked, it is probably inadequate. Recent calculations indicate that while some of the near-edge peaks are indeed attributable to one-electron MO-type transitions whose energies are modified by the presence of the core hole, other features have no such simple origin. Finally we compare the oxide NES of the metal L_{23},K edges and the oxygen K edge altogether. These are found to agree with each other and to MO theory only for TiO_2. The mismatch of the three NES's in the other oxides indicates the failure of one-electron theory for insulators. Instead, the near-edge structure must be dominated by core excitons, as previously shown for NiO. The presence of excitons explains the lack of agreement between the NES for core excitations of different atoms in the same solid.

I. INTRODUCTION

This paper[1] presents results for the K absorption edges of $3d$ transition metals and oxides measured by x-ray absorption spectroscopy (XAS) at the Cornell High Energy Synchrotron Source (CHESS). XAS provides a sensitive probe of the unoccupied conduction states of solids, and this work sets out to explore the information available from an analysis of the data near threshold including comparisons to current theory. Comparisons to previous experimental studies are also made.

First, we review the electron transition probabilities whose variations give rise to the absorption spectra. For XAS, at the energies pertinent to this paper, dipole selection rules apply ($\Delta l = \pm 1$), the $\Delta l = +1$ being by far the most favored in the transitions.[2] The x-ray absorption cross section is written within the one-electron transition model and first Born approximation in terms of a dipole matrix element between an initial core state $\langle i |$ and final state $|f\rangle$ as[3]

$$\sigma_{\text{abs}}(E) = \frac{4\pi^2 e^2}{\hbar c} E \, | \langle f | \vec{e}\cdot\vec{r} | i \rangle |^2 , \tag{1}$$

where E is the photon energy and $\vec{e}$ is a unit vector in the direction of the electric field. (The normalized initial- and final-state wave functions vary as E^{-2}.) In the one-electron (or single-particle) transition model, it is assumed that only one core electron is excited to an unfilled state present in the initial, unperturbed solid. The remaining electrons are assumed to be unaffected, remaining frozen in their original states. Many-body corrections to this picture including relaxation of the valence electrons in response to the core-hole and excited-electron—core-hole interactions alter the one-electron picture; we have discussed this previously.[4] However, if we neglect such effects for the moment, we note that the one-electron cross section may be further decomposed into the product of an energy-dependent matrix element overlap factor $P(E)$ and a projected density of states $N(E)$ with appropriate symmetry[5,6]:

$$I(E) \propto P(E) N(E) . \tag{2}$$

Therefore, the fine structure near the core-edge onset is expected to reflect the density of states obtained from a band-structure calculation, provided that the matrix element factor is slowly varying in that energy region. Calculations for the K and L edges in the $3d$ transition metals indicate that this is

indeed the case.[6–8]

Next we consider the electronic structure and core-edge spectroscopy of the 3*d* transition metals and oxides. The 3*d* transition metals possess narrow partly filled 3*d* bands which give rise to electronic and magnetic properties of physical and technological interest. Figure 1 gives the valence-electron configurations for the metals studied in this paper. We see that the 3*d* band is almost empty in Ti, half full in Cr, and filled in Cu. The one-electron transitions from the core levels to the unoccupied states are shown diagrammatically, and are labeled by the standard spectroscopic notation used herein. Because the initial-state core levels are tightly bound, they have narrow energy widths and little dispersion in k, and are therefore essentially structureless. Hence the core edges are expected to reflect the unfilled conduction-band density of states (DOS) in the solid, as symmetry projected by the dipole selection rule. In the 3*d* transition metals, the DOS near the Fermi level is dominated by the strongly peaked 3*d* states, the *s* and *p* projections being much weaker and diffuse (see Fig. 1). Invoking the dipole selection rule, we expect transitions to the unfilled *d* DOS to dominate the metal L_{23} ($2p \rightarrow d$) core-edge spectra at threshold, as we have verified previously.[4] We have also observed weak dipole-forbidden $3s \rightarrow d$ transitions at large wave-vector transfers in the M_1 edges studied by electron-energy-loss spectroscopy (EELS).[9] On the other hand, the metal K edges measured by XAS presented herein arise primarily from $1s \rightarrow 4p$ transitions, although it appears that the initial features observed at threshold may be due to $1s \rightarrow 3d$ transitions (see below).

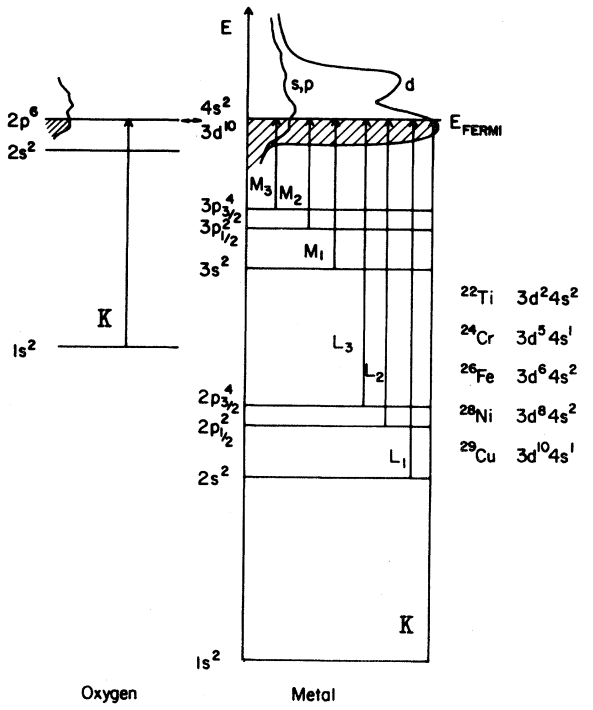

FIG. 1. Core electron excitation diagram for 3*d* transition metals and oxides.

When the transition metals are oxidized, they become insulators, and band gaps of a few electron volts open up between the filled valence and unfilled conduction bands (not shown). Hence the excited electron is poorly screened by the valence electrons from the core hole, spelling the downfall of the one-electron transition model. In some cases, the hole may have a potential strong enough to bind the excited electron. Such a two-particle state is known as a (Frenkel) core exciton and often has an excitation energy below the one-electron threshold. (Frenkel core excitons are highly immobile and may be contrasted to lower-energy Wannier valence excitons in which the excited electron is not localized to the vicinity of the core hole.[10]) With the formation of such core excitons, the dipole selection rule still holds. However, the symmetry-projected final states of the transitions are not those of the unperturbed initial solid. Rather they are determined by the solid containing a partially screened, relaxed core hole.[11] Such a final DOS is *not* expected to be equivalent for excitations (and core holes) centered on different atoms in the same solid. We shall explore this point further during comparisons between our data and one-electron calculations for the DOS and core edges.

The remainder of this paper proceeds as follows. Section II describes the experimental apparatus and samples. The XAS experiments are carried out at the Cornell High Energy Synchrotron Source (CHESS) using the C1 and C2 beam lines which are equipped with tunable Si crystal monochromators. A brief description of the x-ray absorption experiment is given. Core edges from roughly 5–10 keV are recorded at an energy resolution of about 1–2 eV. The samples are either (i) thin metal films or (ii) high-purity chemical powders dusted onto Scotch tape.

Our results for the metal K edges in both the metals and oxides obtained by XAS are presented in Sec. III. The metal-oxide chemical shifts at threshold are compared to those evinced in the metal L_{23} edges. The near-edge structure (NES) is studied and compared to other XAS results. In Sec. IV, we compare the data to single-particle calculations for the K edges in the metals. In Sec. V, we interpret the K NES in the oxides using molecular-orbital (MO) theory, and also review the present state of theoretical calculations, including modifications due to the core hole.

In Sec. VI, we continue our interpretation of the NES in the oxides by comparing the current metal K edges to the metal L_{23} and oxygen K edges measured by EELS for the same compounds and reported previously.[4,12] Using MO theory, we attempt to correlate the NES of these three edges for each oxide. This approach meets with limited success. To explain the failure of one-electron MO theory, we must invoke excitonic contributions to the core edges. Section VII is a summary and conclusion.

II. EXPERIMENTAL

A. Apparatus

X-ray absorption spectra were recorded at 1—2-eV resolution on the C1 and C2 beam lines at CHESS using apparatus designed and constructed by the CHESS staff.[13] Approximately 14 mrad of synchrotron radiation is extracted from the storage ring. Vertical and horizontal adjustable slits then define the beam width and angular divergence incident on the monochromator. The monochromator for the C2 line consists of a channel-cut Si crystal with a weak link. The diffracting surfaces of the crystal are cut parallel to the (220) planes and the monochromator has an energy range of 6 to 30 keV in first order (220). Hence the C2 beam line cannot be used for measurement of the TiK, VK, or CrK edges, although it is suitable for measuring the K edges of the rest of the $3d$ period.

The monochromator on the C1 beam line consists of two independently tunable Si crystals whose diffracting surfaces are cut parallel to the (111) planes. The monochromator operates in a parallel mode, such that the beam is specularly reflected from both crystals. The first crystal intercepts the white beam and is mechanically driven to the appropriate position for each desired energy. The second crystal then intercepts the diffracted beam and redirects it to the sample chamber. This scheme has the advantage of eliminating spurious reflections spatially coincident with the primary diffracted beam. On the C2 beam line, spurious reflections *not* coincident with the primary beam were eliminated by using a second pair of slits.

The energy range of the two-crystal monochromator on the C1 line extends down to 3.5 keV, and so it is possible to measure K edges from the entire $3d$ transition period. On both monochromators, the angle between the two diffracting crystals was detuned for rejection of harmonics having wavelengths λ_{Bragg}/n.

Because the C2 monochromator uses a reflection from planes with smaller d spacing, it has better energy resolution and this result is borne out by experiment. Since fine-structure peak visibility improves with experimental resolution, we shall show Fe, Ni, and Cu NES recorded on C2 line and Ti and Cr NES recorded on C1 line.

Next we present a brief description of the x-ray absorption experiment. The monochromated x-ray beam passes first through a monitor ion chamber, through the absorption specimen, and then into the detector ion chamber. The ratio of detector to monitor ion-chamber currents then provides a measurement of the absorbed fraction of the beam:

$$I_{\text{det}}/I_{\text{mon}} \propto I/I_0 = e^{-\mu_l(E)t}, \tag{3}$$

where $\mu_l(E)$ is the sample linear absorption coefficient which depends on the photon energy E, and t is the sample thickness.

In order to optimize the I/I_0 signal, the gases flowing through the two ion chambers were chosen so that most of the beam passed through the monitor chamber (so that it could impinge on the sample) and to maximize absorption in the detector chamber. For the present experiments, the monitor chamber was 8 cm long and filled with N_2 gas, while the detector chamber was 30 cm long and filled with Ar gas. Using absorption-coefficient data provided at CHESS,[13] one calculates that this arrangement gives 1% monitor-chamber absorption and 95% detector-chamber absorption at 9 keV.

The current signals from the two ion chambers are first amplified by two Keithley 427 current-to-voltage amplifiers. The outputs are then sent into voltage-to-frequency converters and counters whose output is fed into a multichannel scaler for display purposes and also into a Digital Equipment Corporation PDP-11 minicomputer for storage. The computer also drives the monochromator via user-controlled software. Absorption spectra are collected by allowing the monochromator to sit at a given energy for a fixed number of monitor counts while collecting the detector count signal. When the monitor count quota is reached, the counting electronics is rezeroed and the monochromator is advanced to the next energy as determined by the step size. This process is repeated until the desired spectral range has been covered. The practice of using monitor counts to determine dwell time is standard and compensates for fluctuations in beam current from the source.

B. Samples

The samples used in this study were either thin uniform metal films (Ti, Fe, Ni, and Cu) sold by Goodfellow Metals or reagent-grade chemical powders (Cr, TiO_2, Cr_2O_3, FeO, Fe_2O_3, NiO, and CuO) sold by Fischer Scientific Company coated

onto Scotch tape. Diffractometer traces of the commercial TiO_2 powder sample showed it to be anatase phase. Rutile phase TiO_2 powder was produced by heating the commercial TiO_2 to 1100 °C in a furnace for six hours.

For the 3*d* transition metals, the optimum specimen thickness for measuring the *K* edge is roughly $t=1/\mu_l \simeq 4$ μm. For the oxides, a thickness of roughly 12 μm is desired. The metal foils were 4 or 5 μm thick and thus made excellent absorption specimens. Oxide specimens were made by trial and error. Oxide powder was dusted onto Scotch tape until a reasonable absorption step was obtained. This procedure had the disadvantage of creating a nonuniform specimen due to variations in powder-layer thickness, and hence the size of the *K*-shell absorption step was not necessarily that of a specimen with uniform thickness $t=1/\mu_l$. However, for investigation of the near-edge fine structure, such specimens are adequate and commonly used.

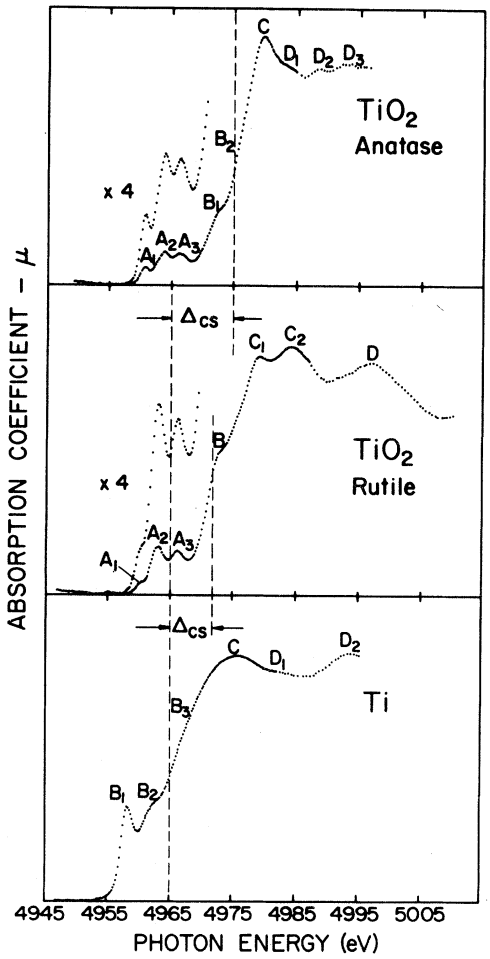

FIG. 2. X-ray absorption *K* edges of Ti in metal and oxides.

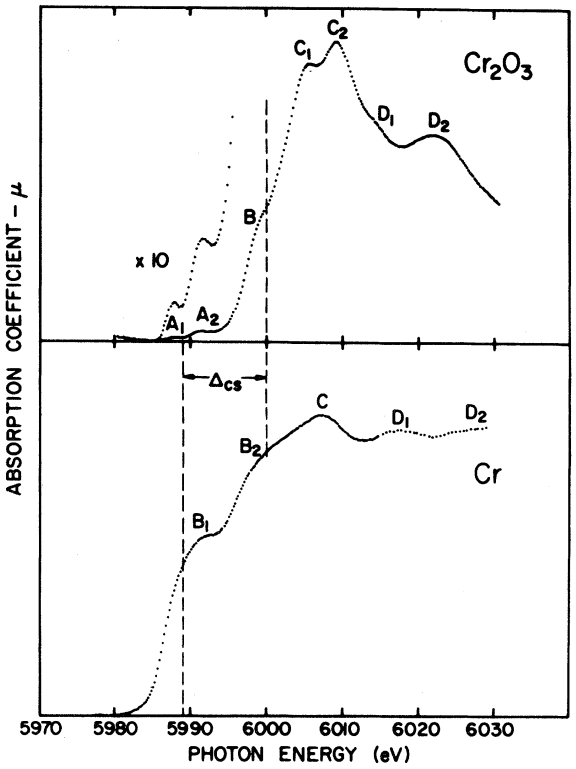

FIG. 3. X-ray absorption *K* edges of Cr in metal and oxide.

III. RESULTS

In this section, we present results for the *K* absorption edges of the 3*d* transition metals and oxides, focusing on the region near threshold. The *K* edges of the 3*d* transition metals and compounds

TABLE I. Chemical shifts between the metal and oxide *K* edges shown in Figs. 2–6. The absolute energies are set by assigning the metal edges to their nearest eV known values (Ref. 27).

Material	*K*-edge energy (eV)	Chemical Shift (oxide minus metal) (eV)
Ti	4965.0	
TiO_2 (rutile)	4971.8	6.8±0.5
TiO_2 (anatase)	4974.8	9.8
Cr	5989.0	
Cr_2O_3	5999.8	10.8
Fe	7111.0	
FeO	7115.1	4.1
Fe_2O_3	7115.8	4.8
Ni	8332.0	
NiO	8332.7	0.7
Cu	8980.0	
CuO	8984.4	4.4

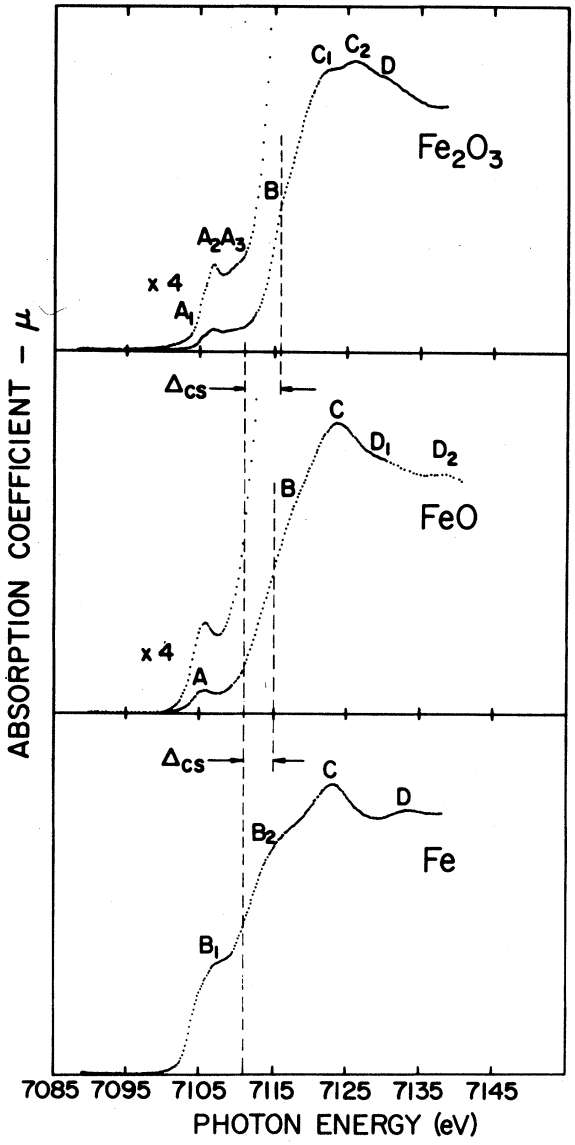

FIG. 4. X-ray absorption K edges of Fe in metal and oxides.

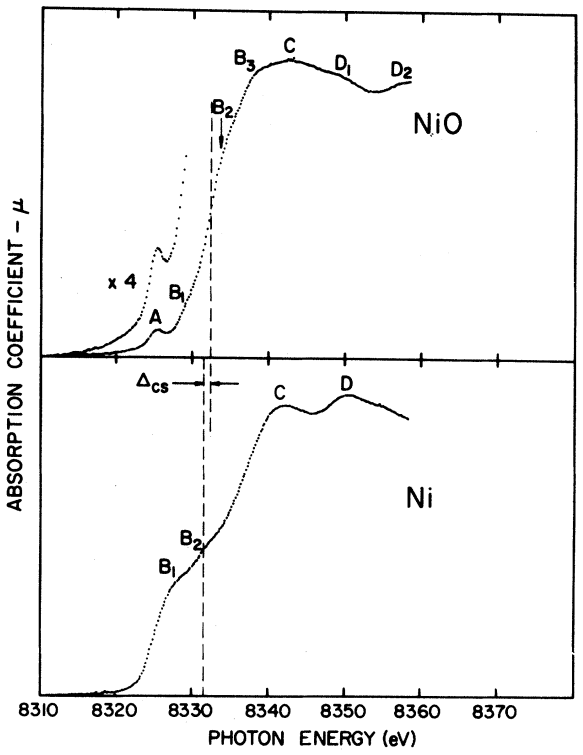

FIG. 5. X-ray absorption K edges of Ni in metal and oxide.

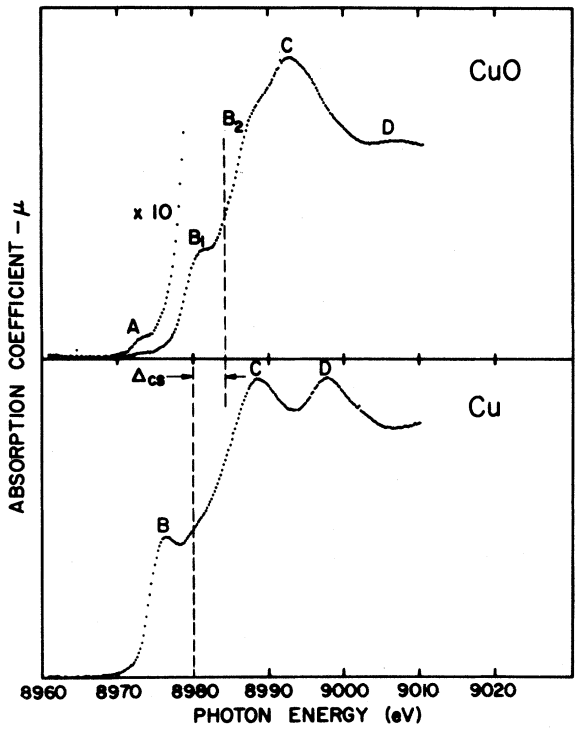

FIG. 6. X-ray absorption K edges of Cu in metal and oxide.

have been the subject of numerous experimental[14–20] and theoretical[7,8,21–26] investigations, and we compare these to our experimental results. The intense monochromated beam flux at CHESS enables one to record spectra with less noise and better energy resolution than previous studies using conventional x-ray tube sources. On the theoretical side, we find excellent agreement between the calculated and measured spectra for the metals, while interpretation of the near-edge structure exhibited in the oxides is presently the subject of intensive investigations.

First, we discuss the chemical shifts and near-edge fine structure of the K edges. Figures 2–6 show the near-edge spectra. The quantity plotted is the linear absorption coefficient, μ_l, which is related

to the ratio I/I_0 of the transmitted to incident beams and the specimen thickness t by

$$\mu_l = -t^{-1}\ln(I/I_0) . \quad (4)$$

In the figures a fine dotted line has been drawn through the point at half the absorption step maximum to denote the edge energy, in keeping with standard practice. The K-edge energies are listed in Table I, in which the absolute energies are set by assigning K edges in the metals to their nearest eV known values.[27] For the oxides, the edge is shifted upward by a chemical shift, Δ_{cs}. This is expected solely on the basis of the shift of the $1s$ core levels, ignoring final-state relaxation effects and the creation of a band gap in the oxides (see Ref. 4). We have previously studied the metal L_{23} edges in these same materials.[4] There we found that these effects caused the oxide edges to lie sometimes at higher energies (TiO_2, Cr_2O_3, FeO) and sometimes at lower energies (NiO, CuO) than for the pure metals. It is presumed that final-state effects also play an inseparable role in determining the chemical shifts in the metal K edges, and we shall not attempt to use them to calculate the charge transfer involved in the core-level shift.

The chemical shifts listed in Table I are much larger than those we have reported for the M_1 (Ref. 9) and L_3 (Ref. 4) edges. However, the percent shift, Δ_{cs}/E_{edge}, is in fact much smaller. This is expected (again ignoring final-state effects) since the tightly bound $1s$ initial-state wave function should be less sensitive than the $2p$ and $3s$ wave functions to changes in the surrounding chemical environment.

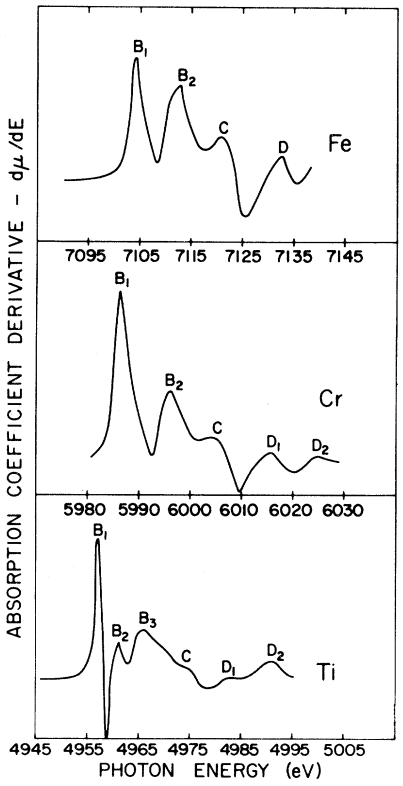

FIG. 7. K-edge derivative spectra for Ti, Cr, and Fe metals.

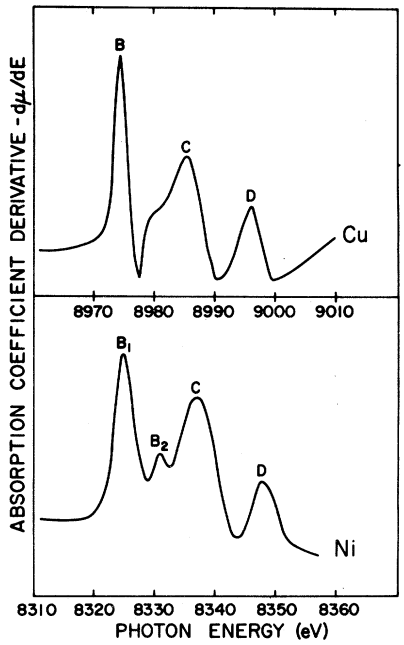

FIG. 8. K-edge derivative spectra for Ni and Cu metals.

Besides the gross increase in absorption at the K-edge step, we also discern in Figs. 2–6 several fine-structure peaks of varying intensities, labeled A–D in each of the spectra. These secondary peaks are more visible in the derivative curves shown in Figs. 7–10, which were drawn through points given by

$$\frac{d\mu_l}{dE} = \frac{\mu_l(E+\Delta)-\mu_l(E)}{\Delta} , \quad (5)$$

with Δ the step size of the spectrum. For the metals, the derivative spectra enhance the humps (B) leading up to the absorption maximum (C) which is followed by additional peaks (D). In a one-electron interpretation, these features are expected to reflect peaks in the unfilled p density of states (DOS), and we discuss this further in Sec. IV. Upon oxidation, very weak but sharp peaks (A) appear several eV below the main absorption step; these are also enhanced in the derivative spectra, and have been widely attributed to dipole-forbidden $1s$-to-$3d$ transitions. We note that in CuO, the A pre-edge peak is especially weak. This is consistent with our previous observation[4] that the CuO L_{23} white lines were also much weaker than the white lines of the transi-

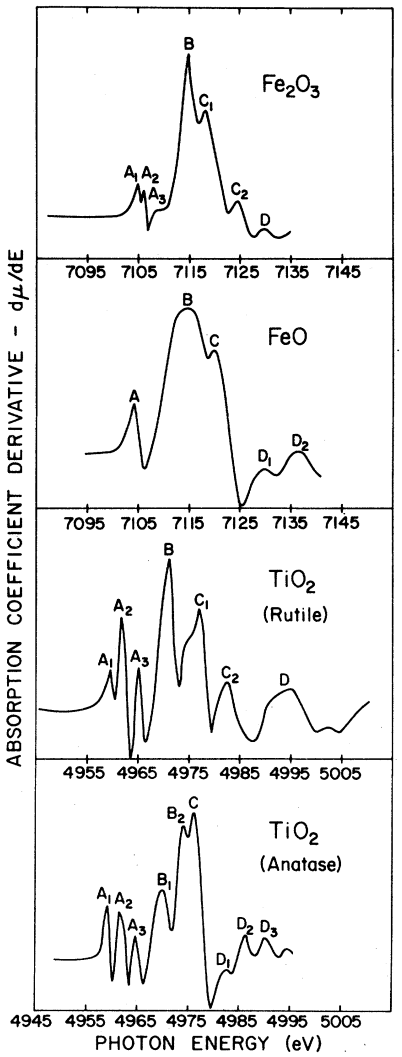

FIG. 9. K-edge derivative spectra for oxides of Ti and Fe.

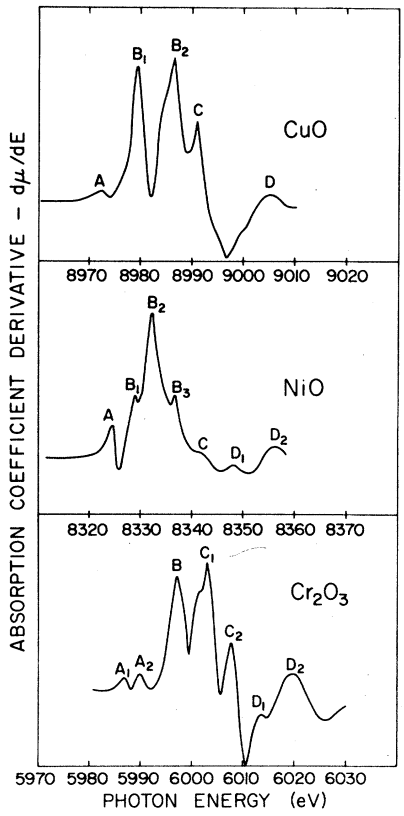

FIG. 10. K-edge derivative spectra for oxides for Cr, Ni, and Cu.

tion metals and oxides. The L_{23} edges arise from $2p$-to-$3d$ transitions, while Cu metal has a full $3d$ band. Presumably, in CuO, only a narrow slice of the $3d$ DOS is unfilled, weakening the net $2p$-to-$3d$ transition strength. Therefore, the observation that the present pre-edge peak A is also weaker in CuO than in the transition-metal oxides corroborates the $1s$-to-$3d$ interpretation of its origin.

Before continuing, we note the variations observed between oxide spectra of the sharpness of the absorption step maxima (C) and also the rate at which the absorption spectra tail off. This is due in part to variations in the thickness between oxide specimens, which unlike the metals were not uniform foils, but rather fine ground powder dusted onto Scotch tape. Thicker dustings produced rounded absorption steps (e.g., NiO) while thinner dustings produced sharp absorption steps followed by a rapidly decaying tail (e.g., Cr_2O_3, CuO). This type of behavior is well known in x-ray absorption and is termed the "thickness effect."[28] In the present work, we shall be concerned primarily with the positions of the oxide NES peaks and not so much with their relative sharpness, and so we need not be concerned here with separating out thickness effects.

The measured K absorption spectra in Figs. 2—6 may be compared to those published by other investigators. Early results were obtained using the bremsstrahlung radiation from rotating anode x-ray sources and were hampered by a lack of source intensity. Newer studies using monochromated synchrotron radiation are generally characterized by better signal to noise covering a larger energy range, due to the 5 orders of magnitude increased intensity of synchrotron over conventional sources.

Until recently, some of the best x-ray absorption K-edge spectra for $3d$ transition metals were those recorded by Beeman *et al.* in 1939.[14] Considering the weakness of their source, the quality of their spectra is astounding. Their spectra for Fe, Ni, and Cu are virtually identical in shape to ours and display all our B, C, and D fine-structure peaks (Figs. 4—6) with the exception of the weak B_2 peak in Ni, which is missing due to their more widely

spaced data points. Newer data of Smulowicz *et al.*[23] displays both B_1 and B_2 Ni peaks. Spectra by Tsutsumi *et al.*[16] for Ti and Cu also show all B and C maxima labeled in our data. All three studies[14,16,23] were carried out using conventional x-ray sources.

For the oxides, previous conventional source spectra generally have insufficient resolution and statistics to resolve the fine structures observed herein. Often missing are some or all of the weak, sharp peaks (A) of the secondary maxima (B),[15–17] although with care and patience, sufficient signal and resolution to resolve all these features is possible.[18] New synchrotron-radiation fluorescence studies of rutile and anatase TiO_2 by Sandstrom *et al.*[20] show all three A peaks in agreement with the present data. Also, Belli *et al.*[19] have published synchrotron-radiation absorption spectra for various Mn oxides displaying fine structure closely resembling our results. Finally, we note that all of the above oxide specta[15–20] display line shapes in good agreement with the present data.

IV. COMPARISON BETWEEN METAL K-EDGE FINE STRUCTURE AND SINGLE-PARTICLE CALCULATIONS

In this section we compare our experimental results for the K edges in the metals with those predicted by theory within the single-particle or one-electron transition model. Several authors have calculated $3d$ transition-metal K edges[8,21–24] including various broadening schemes and we consider each work in turn. We find that the locations of the spectral maxima are well predicted by theory, although it appears that intensity discrepancies in the near-edge region may be ascribed to the neglect by theory of many-body effects.

The best systematic calculation for the $3d$ transition-metal K edges is that of Müller, Jepsen, and Wilkins.[7] Using a linearized augmented-plane-wave method, these authors have calculated the $3d$ transition-metal K edges including both initial- and final-state (or "hot-electron") broadening effects. Excluded are experimental resolution and many-body effects, including neglect of the core hole and relaxation of the valence electrons in response to the hole (see, e.g., Ref. 4).

In Fig. 11, we fit our experimental results with the calculation of Müller *et al.* In keeping with the procedure proposed by Materlik *et al.*,[29] we artificially compress the experimental energy scale of our data. Hence the experimental data is plotted with an abscissa given by the ratio of E to the compression factor (CF), where E is the relative energy above onset. Table II lists the empirically determined values for CF. Slight differences in CF between spectra acquired on the C1 and C2 beam lines are most likely due to miscalibration and/or human error in fitting the curves. These compression factors are roughly equal to those employed by Materlik *et al.* in their comparison of the same one-electron theory with experiment for the L absorption spectra of the rare-earth metals.[29]

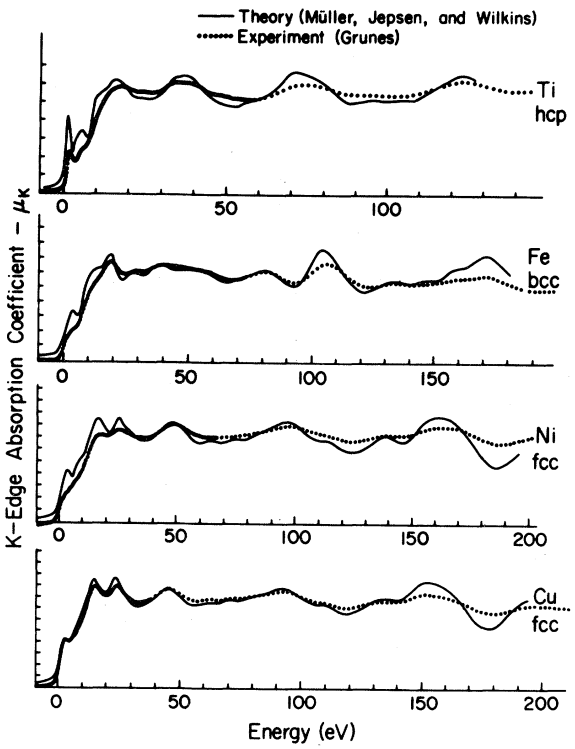

FIG. 11. Calculated and measured K absorption edges over an extended energy range for selected $3d$ transition metals. (Calculated edges from Ref. 7.)

While the reason for compressing the energy scale of the data to match the calculation is unclear, there are several developments[29,30] pointing to the importance of the core hole. First, Herbst and Wilkins[30(a)] have previously found it necessary to include complete relaxation of the core hole to obtain agreement

TABLE II. Empirically determined scale compression factors (CF) used in Fig. 11 to fit the experimental data to single-particle calculations by Müller *et al.* (Ref. 7). Plotted experimental energies relative to the edge onset have been divided by CF. Underlined CF values identify source for experimental spectra plotted in Fig. 11.

Metal	CF (C1 beam line)	CF (C2 beam line)
Ti	<u>1.05</u>	
Fe	<u>1.07</u>	1.05
Ni	<u>1.07</u>	1.04
Cu	1.05	<u>1.02</u>

with photoemission binding-energy data. Second, the work of Noguera[30(b)] and collaborators on the dynamic screening of the core hole suggests that for energies near threshold, the effective potential is that of the fully screened core hole while for energies far above threshold, the effect of screening is much weaker. This effect might alter the high-energy part of the calculation. Clearly, more theoretical work is needed.

Returning now to Fig. 11, we are struck by the remarkably close agreement between theory and experiment, illustrating the success of a careful single-particle calculation in predicting the relative position and intensity of every peak and valley in the metal K absorption edges out to 200 eV above threshold. However, near threshold, we do note some interesting discrepancies. For example, the calculated spectra for fcc Ni and Cu are virtually identical in shape (after appropriate energy-axis rescaling for differences in lattice spacing).[7] This is not so for the experimental data near threshold, most clearly seen in the NES Figs. 5 and 6 where we see that the initial peaks B, C, and D are more prominent in Cu. The suppression in Ni versus Cu of these features is readily apparent in Fig. 11, where the Cu near-edge data match the calculation much more closely than for Ni. A similar suppression of experiment versus theory in the near-edge region is observed for Ti and Fe. Notice too that the initial maxima in Ti and Cu are equally sharp in experiment and theory. This suggests that the theory curves have been sufficiently broadened to match the present experimental resolution. (This is plausible, since the initial-state width values used to broaden the theory have a significant experimental uncertainty, roughly equal to our present resolution.)

The suppression in our data of the calculated initial spectral maxima in Ti, Fe, and Ni may be due to neglected many-body effects which are known to alter the line shapes near threshold. For example, Citrin *et al.*[31] have carefully investigated the many-body effects for the K and L_{23} absorption edges of Li, Na, Mg, and Al. By including processes such as phonon broadening and the Mahan—Nozières—De Dominicis many-body response of the conduction electrons in their calculated edges, they find that the K edges are rounded and the L_{23} edges enhanced near threshold, yielding excellent agreement with experiment. Similar many-body corrections to the spectra of Müller *et al.*[7] might also improve the present match with experiment.

Next we consider the origins of the fine structure observed in the calculated and measured K edges. Since this structure is calculated within the dipole approximation, it must be due to peaks in the unoccupied p DOS, including hybridization of the p bands with bands of different symmetry. Although Müller *et al.*[7] identify the lowest-energy peak in each of the K edges as due to a transition to the narrowing unfilled portion of the $3d$ band, they do not identify the transitions involved in further maxima. Work is currently in progress by Müller and Schaich to identify the origins of the remaining structures.[32]

Finally, we note that the present agreement between our data and the calculations of Müller *et al.*[7] is much closer than previously reported for the metal L_{23} edges, which were measured by electron energy-loss spectroscopy (EELS).[4] Figures 12 and 13 show the two sets of L_{23} edges in which the dashed theory curves are from Ref. 7. (These differ slightly from the preliminary curves for Ni and Cu which appeared in our previous report.[4]) The calculated spectra are scaled vertically to match the data at the L_2 edge. While a good fit between theory and experiment is found for Fe, Ni, and Cu, in Ti and Cr the measured L_3 white line is much weaker in intensity than theory predicts. Further, as found for the K edges of the adjacent fcc lattices Ni and Cu,

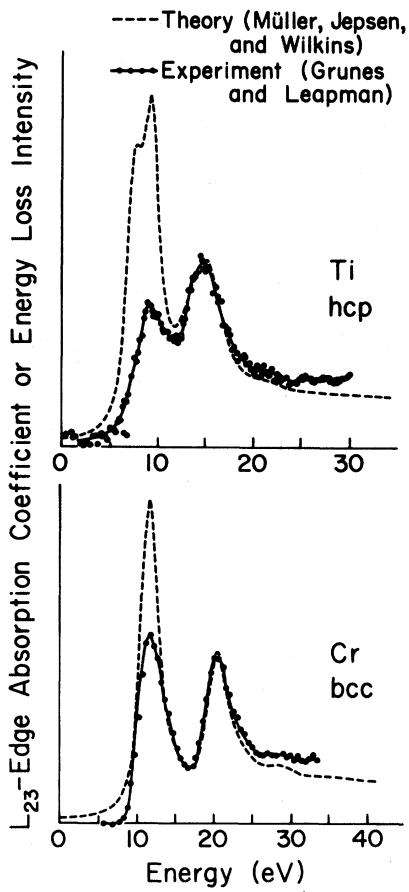

FIG. 12. Calculated and measured L_{23} edges for Ti and Cr scaled vertically to match at the L_2 edge. (Calculated edges from Ref. 7.)

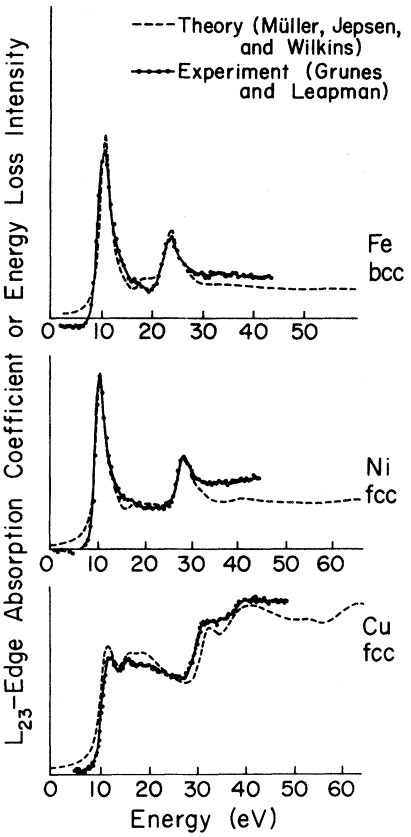

FIG. 13. Calculated and measured L_{23} edges for Fe, Ni, and Cu scaled vertically to match at the L_2 edge. (Calculated edges from Ref. 7.)

the calculated L_{23} spectra for the adjacent bcc lattices Cr and Fe are virtually identical in shape (again after appropriate energy rescaling for differences in lattice spacing).[7] Such is not the case for the EELS data—the Fe L_3/L_2 intensity ratio is obviously greater than that of Cr.[4] This discrepancy may also be a many-body correction neglected by the one-electron calculation, although currently there is no adequate explanation.

The K absorption spectra of the $3d$ transition metals with neglect of the core hole have also been calculated by Smulowicz *et al.*,[23] Nagel *et al.*,[8] and Wakoh *et al.*[22] Smulowicz *et al.*[23] have calculated the Ni K edge out to 40 eV above threshold, and assign the spectral maxima to peaks in the DOS associated with bands of mostly p character (in keeping with the dipole selection rule). In Fig. 14 we show their calculated Ni K edge, which has been broadened by an initial-state Lorentzian, final-state broadening having been neglected. Also shown are the present experimental results from Fig. 5, which are quite similar to the experimental data of Smulowicz *et al.* Because of the limited-energy range involved, it was not found necessary to rescale the ex-

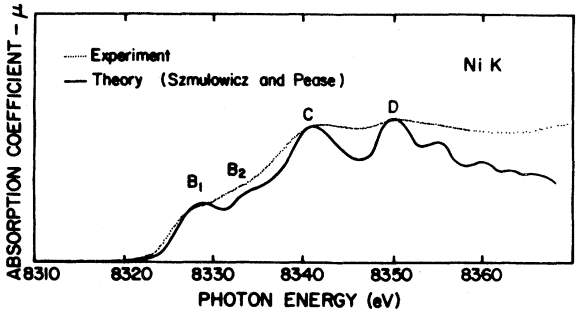

FIG. 14. Calculated and measured Ni K absorption edge. (Calculated edge from Ref. 23.)

perimental energies as was done in Fig. 11. We see in Fig. 14 that the positions of the first four maxima, labeled B_1, B_2, C, and D, are in good agreement, and also that these peaks are once again more prominent in the calculation. (The straggling tail of the theory curve is ascribed to the neglect of higher-energy bands which contribute to the spectrum at lower energies through hot-electron broadening.[23]) Smulowicz *et al.* observe that hot-electron broadening cannot explain the suppressed B_1 peak in the data at onset, since this broadening mechanism goes to zero at the Fermi energy, where the onset of absorption occurs. They estimate that phonon broadening is also an insufficient cause. Their conclusion is consistent with our comparison above to the calculation of Müller *et al.*[7] Smulowicz *et al.* state that "a careful one-electron band calculation, neglecting the effects of the core hole in the crystal, yields excellent agreement with the observed Ni K edge except near threshold where the experimental spectrum is without doubt somewhat rounded relative to the one-electron crystal calculation."[23]

The Ni K absorption spectrum out to 25 eV above threshold has also been computed by Nagel *et al.*,[8] again neglecting the core hole, but including initial and hot-electron broadening. The resulting spectrum is quite similar to that of Smulowicz *et al.*[23] and we need not consider it in detail. Finally, Wakoh *et al.*[22] have computed the K edges for V, Fe, Ni, and Cu including initial-state Lorentzian broadening. Since they used fewer k points in their mesh, their results are not as accurate as those of Müller *et al.*[7] Nonetheless, the gross features of the calculated spectra of Wakoh *et al.*[22] can also be matched to the experimental data. Once again, we find that the peaks near threshold are more prominent in theory than in experiment for all but Cu, for which good agreement is observed.

In summary, single-particle (one-electron) calculations with neglect of the core hole do well in predicting the spectral features observed in the $3d$ transition-metal K edges. Relatively small discrepancies between theory and experiment near

threshold are most likely caused by the neglect of many-body effects while the slight rescaling necessary to fit theory and experiment over an extended energy range may be possible to correct by including electron relaxation in response to the core hole. As we shall soon see, the absorption spectra of insulators, including $3d$ transition-metal oxides, are not nearly so well understood.

V. INTERPRETATION OF OXIDE NEAR-EDGE STRUCTURE WITH COMPARISONS TO THEORY

In this section, we review the empirical and theoretical interpretation schemes for the near-edge structure (NES) observed in the oxide spectra (Figs. 2—6). Because these oxides are insulators, the core hole left behind in an excitation is incompletely screened, unlike in metals where the screening is good. Therefore, many-body effects involving both the core hole and the excited electron are expected to be more important for the oxides. Single-particle calculations have been less successful at predicting their NES and no detailed quantitative agreement between experiment and theory has yet been achieved. Instead, we content ourselves with a description of the progress to date.

Glen and Dodd[15] were among the first to use molecular-orbital (MO) theory to explain the K NES of various transition-metal complexes. MO theory denotes here a symmetry-based model for a cluster consisting of a metal atom surrounded by its oxygen nearest neighbors. In the oxides whose spectra are shown in Figs. 2—6, each atom is octahedrally coordinated to its six nearest-neighbor oxygen atoms (four in the basal plane and one each above and below). By considering the symmetries of the metal-ligand atomic orbital pairings, a MO energy-level hierarchy is deduced. Figure 15 shows such an energy-level diagram[16] with valence-electron occupancies for the $(TiO_6)^{8-}$ cluster representing the environment around Ti in TiO_2. The level spacings are as yet unknown, since symmetry considerations alone cannot yield quantitative energies. This same level hierarchy also applies to the octahedral metal-oxygen clusters found in the rest of the oxides listed in Table I, the only difference being the increase in the number of filled orbitals as the metal-ion atomic number increases. Accepting this picture, one assigns peaks in the core-edge NES to transitions to the unoccupied MO's. Transition strengths should be governed by dipole selection rules. Hence in the metal K edges, transitions to the $2t_{2g}$ and $3e_g$ orbitals of mostly $3d$ character are expected to be much weaker than the dipole-allowed transitions to the $4t_{1u}$ orbitals of mostly $4p$ character.

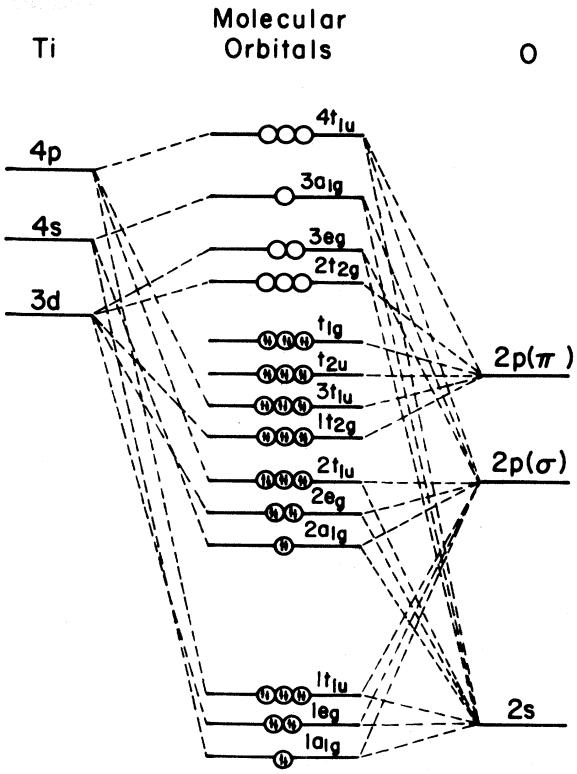

FIG. 15. Molecular-orbital energy-level diagram with electron occupancy for $(TiO_6)^{8-}$, representing the octahedral coordination about Ti in TiO_2. The same diagram with different electron occupancies applies to the rest of the oxides listed in Table III. (Figure from Ref. 16.)

Glen and Dodd's[15] K-edge spectra display three general near-edge features corresponding to peaks A, B, and C in Figs. 2—6. Using the above MO scheme, they assign these features to one-electron transitions. The A peak(s) are weak quadrupole $1s$-to-$3d$ excitations involving transitions to the $2t_{2g}$ and $3e_g$ MO's. (For energies above a few keV, nondipole terms begin to contribute to the absorption cross sections.) Evidence for this assignment comes from the observation[15] that the A peak(s) are much stronger in tetrahedrally coordinated complexes than in complexes which are octahedrally coordinated. While the octahedral coordination has an inversion center of symmetry, the tetrahedral coordination does not. Therefore, in the latter case, the ligand field breaks the spherical symmetry of the atomic potential. This distortion changes evaluation of the transition-matrix integral, and in effect relaxes the dipole selection rules. Hence we expect an increase in the strength of $1s$-to-$3d$ quadrupole transitions in tetrahedral versus octahedral compounds, and the A peak(s) display this behavior. (The result that dipole selection rules hold only in systems with an inversion center is known in optical spectroscopy as

Laporte's rule.[33])

The weak humps corresponding to the B peak(s) in Figs. 2–6 leading up to the absorption maximum, are identified[15] as monopole 1s-to-4s transitions to the $3a_{1g}$ MO's. (We shall find below that this is probably incorrect.) Finally, the main absorption maximum (C) is identified as the dipole 1s-to-4p transition to the triply degenerate $4t_{1u}$ MO's. Glen and Dodd explain any further peak splitting as evidence of a splitting of the degenerate antibonding orbitals due to asymmetric metal–ligand bonding. Their assignment scheme is directly applicable to our oxide spectra and we shall adopt, for the present, their explanations for the A, B, and C peaks evinced in our spectra.

The MO scheme has also been used by Shulman *et al.*[34] to explain the x-ray absorption near-edge structure found using absorption of synchrotron radiation in various Fe compounds and proteins. Their K edges also display the three NES peaks A, B and C, and the same MO assignments described above are invoked to explain their occurrence. Shulman *et al.* also attempt to quantify their interpretations by comparing the measured NES peak spacing in the ionic perovskite cubic fluorides (KXF_3, where X=Mn, Fe, Co, Ni, and Zn) with atomic calculations for the unoccupied levels for the $Z+1$ atom. (The $Z+1$ approximation is a crude way of taking into account the tightly bound 1s core hole.) The measured peak spacings are in good agreement with the atomic calculations. Also the weak peak A appears in all but the Zn $3d^{10}$ salt spectrum, a further evidence for its 1s-to-3d assignment.

Other investigators using the MO approach include Sugiura *et al.*,[18] who assign the same transitions as above to the NES of octahedrally coordinated transition-metal compounds, and Ichikawa *et al.*,[17] who measured the NES of Cr, Mn, Fe, and Co compounds. Ichikawa *et al.*[17] find fair agreement between the empirical MO spacings as deduced from the NES peaks in K_2CrO_4 and MO energy-level spacings for CrO_4^{2-} calculated by Viste and Gray.[35] The fit to the calculated $Z+1$ spacings for MnO_4^{2-} was poorer. Tsutsumi *et al.*[16] also assign MO transitions to their Ti K spectrum in rutile TiO_2, labeling peaks B and C as transitions to $4t_{1u}$ and $5t_{1u}$ ($4p$,$5p$) MO's.

More recently, Belli *et al.*[19] have published a careful synchrotron-radiation absorption study for the NES of Mn K edges in simple oxides and complex compounds in which the Mn atom is octahedrally coordinated. First they show the NES of complex Mn compounds in which the Mn atom is octahedrally coordinated. Because these compounds exhibit poor long-range order, one presumes that solid-state contributions to the NES are minimized, i.e., the final-state wave function is determined primarily by the potential of the local molecular cluster. Here they find good agreement between their experimental NES peak separations and Tossell's[36] calculated MO levels for the $Z+1$ cluster $(FeO_6)^{10-}$. Based on the calculations, they assign the NES peaks corresponding to our peaks A–D in Figs. 2–6 as follows: The weak A_1 and A_2 pre-edge peaks are transitions to the $2t_{2g}$ and $3e_g$ MO's of primarily Mn 3d character, and the pre-edge hump, B, is a transition to the $4t_{1u}$ MO of mostly Mn 4p character. The main absorption maximum (C) is not a MO transition, but rather a "shape resonance." At the "resonance energy," the final-state wave function is confined inside the $(MnO_6)^{9-}$ molecule by the effective combined Coulomb plus centrifugal barrier potential, the latter acting more strongly on the high-l components of the final-state wave function. We have previously observed a similar delayed-onset centrifugal-barrier effect in the Nb M_{45} edge.[37] The M_{45} edge is a d-to-f symmetry transition, and hence one expects the observed barrier effect. The like assignment of a peak in the 1s ($l=0$) absorption spectrum is more controversial. Finally, Belli *et al.* assign the post-maximum peak D to "delocalized states." In keeping with this interpretation, the position of peak D is found to be sensitive to differences in the second coordination shell between compounds.

Notice that Belli *et al.*[19] differ from the previous investigators in their assignment of the transitions involved for the B and C peaks. Belli *et al.* assume that the 1s-to-4s transition is too weak to be observed and instead assign peak B as a 1s-to-4p transition, while the other studies assigned the transition to peak C. MO energy-level spacing calculations are cited as evidence for both assignments. Clearly, more sophisticated calculations including transition strengths are necessary, and we shall consider two examples below.

Having looked at the NES of the Mn K edge in solution and molecular complexes, Belli *et al.* next consider the NES of the octahedrally coordinated oxides MnO, Mn_2O_3, and MnO_2, which exhibit strong long-range order and have crystal structures similar to the oxides measured in this paper. Although the usual A, B, C, and D structures are present in all the spectra, the splittings and spacings of these peaks are not explainable using MO theory. Specifically, Mn and MnO_2 have very similar octahedral nearest-neighbor environment, yet their NES's are quite distinct. Belli *et al.*[19] conclude that although the same MO transition assignments may still be qualitatively correct for the oxides, solid-state effects must come into play. Hence the MO approach is not sufficient, and one must consider long-range order (i.e., more atoms than a simple

cluster) to describe the final-state wave function for the Mn oxides, and by inference, for the $3d$ transition-metal oxides whose spectra we have measured.

The above five studies were primarily experimental in nature. Comparisons were made only to calculated MO energy-level spacings; no transition strengths were included. However, more quantitative calculations for the NES in transition-metal complexes are currently being pursued, and a few results published. Bair *et al.*[25] have carried out *ab initio* self-consistent-field calculations on the excited states of the $CuCl_2$ molecule involving excitations of the Cu $1s$ orbital into bound valence and unbound virtual orbitals. They calculate both the absolute excitation energies and also the transition strengths, and include the presence of the fully relaxed core hole. The $CuCl_2$ edge displays the usual A, B, and C maxima (see Figs. 2—6). They find that the weak pre-edge peak A is indeed due to a transition to a MO of primarily metal $3d$ character, in agreement with the above studies.[15—19,34] The main absorption maximum C is assigned as a transition to MO's of primarily metal $4p$ character, in agreement with some of the above studies.[15,18,34] However, the shoulder B is not assigned to any single-electron transition. The $1s$-to-$4s$ monopole transition strength is found to be far too weak to be observed and appears at the wrong energy to fit the B-peak data. Rather, this feature is reassigned as a $1s$-to-$4p$ MO transition plus simultaneous shakedown. The calculation shows that when the $1s$ electron is removed and the system permitted to relax, the ground state changes from $3d^9$ in $CuCl_2$ to $3d^{10}$ in $CuCl_2^+$. The electron filling the additional d orbital comes from one of the highest-occupied ligand orbitals ($4p\sigma$ or $4p\pi$). Shakedown transitions are, of course, ignored in one-electron transition schemes since these neglect system relaxation in the presence of the core hole. The $Z+1$ approximation to the core hole invoked above is also incapable of handling such multielectron events.

Bair *et al.*[25] expect their results to hold for other transition-metal complexes. Hence, according to their study, the B peak(s) observed in our $3d$ transition-metal oxides are due to $1s$-to-$4p$ shakedown transitions from different ligand orbitals.

Similar calculations have been undertaken by Kutzler *et al.*,[26] who have completed first-principles self-consistent-field $X\alpha$ calculations for the NES of various molecular clusters, including chromate (CrO_4^{2-}) which is tetrahedrally coordinated. Like Bair *et al.*,[25] they calculate the one-electron transition strength into bound and continuum states including the fully relaxed core hole. Their transition assignments for the pre-edge peak A and the main absorption maximum C are essentially the same as those of Bair *et al.*: Peak A is due to transitions to a bound state of mostly $3d$ character and C is due to continuum $1s$-to-$4p$ transitions. Again, $1s$-to-$4s$ transitions are computed as too weak to be observed. Rather the shoulder B is found to be an inherent feature of continuum transitions. However, we note that the results of Kutzler *et al.*[26] fail to predict the various B-shoulder peak splittings observed in the measured spectra. They speculate that many-electron processes (such as the shakedown transitions calculated by Bair *et al.*[25]) may be involved but do not attempt to incorporate such effects into their calculations.

From the above studies, we see that interpretation and calculation of the NES for insulating compounds is much less clear-cut than for the metals (see Sec. IV). Many-electron effects due to an incompletely screened core hole appear to be sufficiently important to alter the simpler MO transition scheme invoked by various investigators. Although it appears that we are safe in labeling the pre-edge peak(s) A and main absorption maximum C as $1s$-to-$3d$ and $1s$-to-$4p$ MO transitions, respectively, more corroborating calculations are needed before a definite assignment of the peaks B and D is possible. An eventual goal of the NES calculations, viz., to identify the structure of unknown dilute compounds, is distant.

VI. CORRELATION OF THE METAL K, L_{23}, AND OXYGEN K NEAR-EDGE FINE STRUCTURES FOR THE OXIDES

In this section we complete our discussion of the near-edge structure (NES) of the oxide core-edge spectra by applying the ideas developed in Sec. V to the interpretation of three measured edges in each material. To do this, we attempt to correlate the NES peaks evinced in the metal L_3 (Ref. 4), metal K (the present study), and oxygen K (Ref. 12) edges. In a one-electron transition model, such peaks arise from excitations to peaks in the conduction-band density of states (DOS). If one assumes that the slowly-varying, energy-dependent matrix-element factor affects only the strengths and not the positions of the spectral features, then there should be a one-to-one correspondence between peaks in the DOS and the measured spectra.[38] Hence we should be able to line up our three measured edges so that the features match. In the absence of a band-structure calculation extending to the unoccupied states for the oxides, we resort instead to the molecular-orbital (MO) theory introduced in Sec. V and attempt to assign spectral peaks as transitions to virtual MO levels. Although we achieve limited

success, our general failure must be attributed to severe many-body alterations of the NES. The oxides considered in this paper are all insulators. Therefore, the valence charge is localized and cannot effectively screen the excited electron from the core hole. In some cases, the electron and hole form a two-particle bound state, or core exciton, and propagate together in the crystal.[10,38–41] The final-state energies for core excitons can lie inside the valence- to conduction-band gap, creating new spectral peaks below the onset of one-electron core level to conduction-band transitions. Core excitons can also exist within the conduction-band continuum, contributing to the spectral features above the one-electron transition threshold. Alternately, the excited electron and hole can scatter elastically from each other, drastically changing the strength of the one-electron transitions while leaving their energies intact.[38] The strength of these excited-electron—core-hole interactions varies for excitations of different atoms in the same solid, and hence if such many-body effects cannot be neglected, no NES correlation is expected.

We have previously reported an attempt to match the same three core near-edge fine structures for rutile TiO_2 and CuO,[12] using conventional source x-ray absorption metal K edges measured by Tsutsumi *et al.*,[16] and our metal L_{23} and oxygen K edges measured by EELS.[4,12] (Calculations by collaborating theorists for rutile TiO_2 and the NiO oxygen K edge were also presented, and the interested reader is referred to this earlier paper.[12]) Since then, the low-noise, high-resolution metal K edges shown in Figs. 2–6 have been measured, covering all the oxides previously studied by EELS. Our new spectra display features not previously discerned in the spectra of Tsutsumi *et al.*[16] However, we shall find that the main conclusion of our previous study, viz., that one-electron MO theory cannot adequately describe the spectra of most $3d$—transition-metal oxides, still holds.

We begin by applying MO theory (Sec. V) to all three core edges measured for each material and return to the MO energy-level diagram appropriate to these octahedrally coordinated complexes shown in Fig. 15. The valence-electron occupancy is filled in for the $(TiO_6)^{8-}$ cluster representing the nearest-neighbor environment about Ti in TiO_2. In the case of $(TiO_6)^{8-}$, we see that the 48 valence electrons completely fill the π- and σ-bonding orbitals containing mostly oxygen $2p$ character, leaving unfilled the antibonding orbitals $2t_{2g}$ ($d\pi^*$) and $3e_g$ ($d\sigma^*$) containing mostly Ti d character. The $2t_{2g}$ and $3e_g$ levels are also unfilled in $(CrO_6)^{10-}$, while only the $3e_g$ level remains unfilled in the Fe, Ni, and Cu octahedral clusters. Accepting this picture, one can

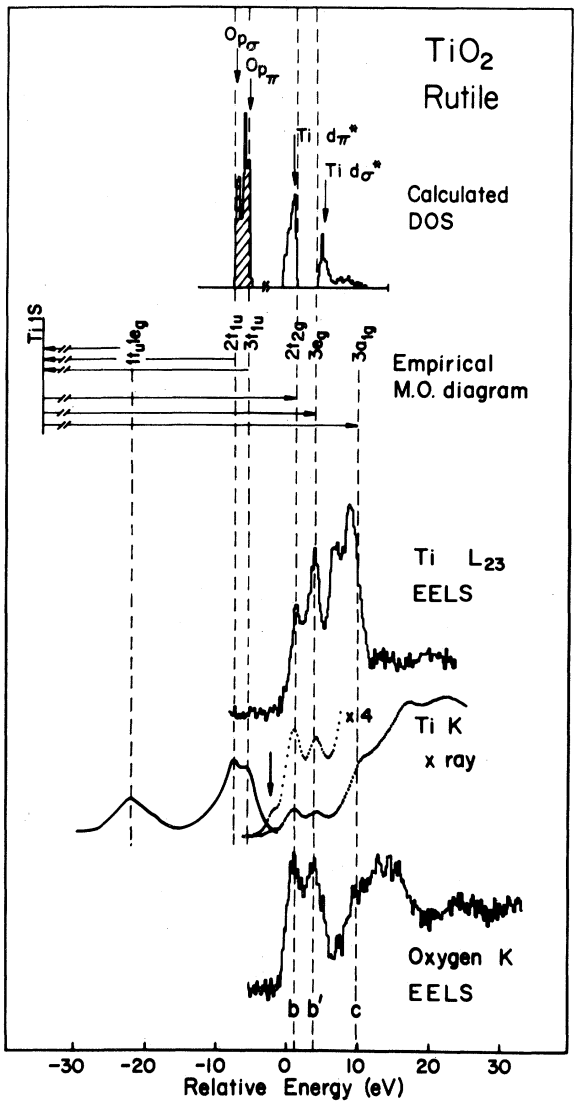

FIG. 16. Fine-structure peaks in the Ti L_{23}, Ti K, and O K edges in TiO_2 are aligned to construct an empirical MO energy-level diagram. The energy-level spacings are in good agreement with peaks in the calculated conduction-band DOS of Wilker and Hoffmann (Ref. 12). (The Ti K emission data at negative energies is from Ref. 16. EELS data from Refs. 4 and 12.)

deduce the MO energy-level spacings directly from the NES's on the core edges. Invoking the dipole approximation, $\Delta l = \pm 1$, appropriate to XAS or small scattering angle EELS, we consider metal L_3 ($2p_{3/2} \rightarrow$ mostly d states around the metal atom), metal K ($1s \rightarrow p$ states around the metal atom), and oxygen K ($1s \rightarrow p$ states around the oxygen atom) excitations. These three edges are aligned at threshold in Figs. 16–20 for TiO_2, Cr_2O_3, FeO, NiO, and CuO. In Table III, we list the NES peak energies relative to the initial peak which is taken to corre-

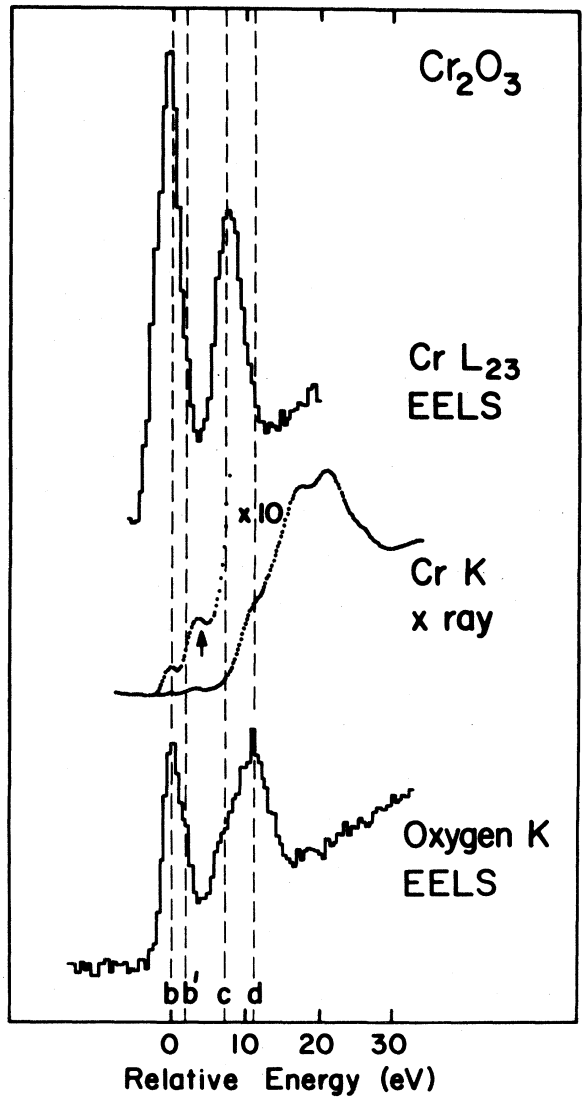

FIG. 17. Alignment of fine-structure peaks for three core edges in Cr_2O_3. Fine structure above the Cr L_3 edge is obscured above 9 eV by L_2 edge onset. (EELS data from Refs. 4 and 12.)

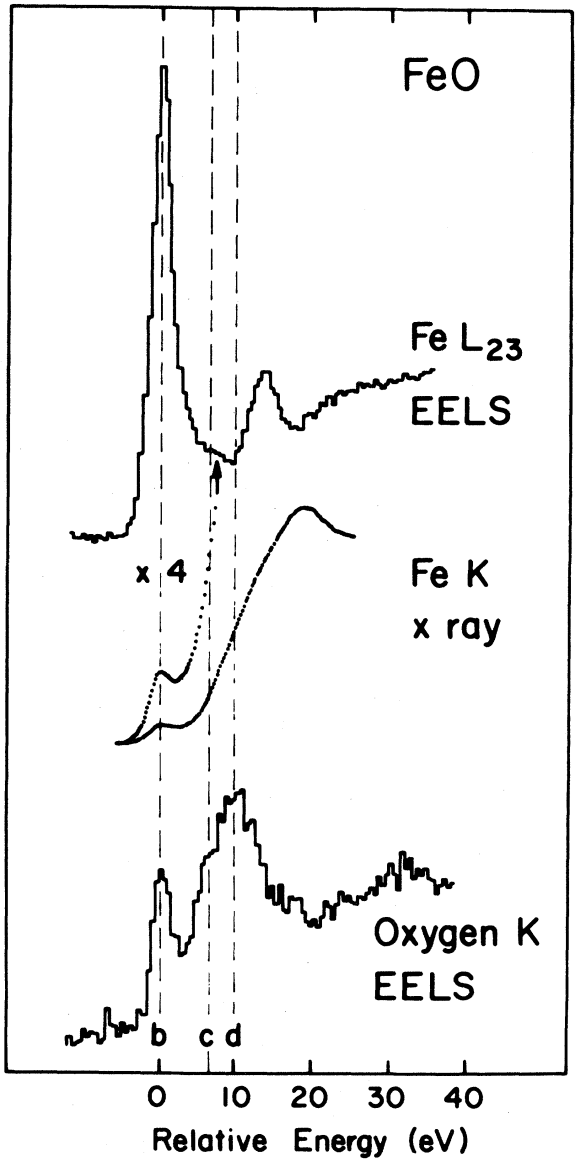

FIG. 18. Alignment of fine-structure peaks for three core edges in FeO. (EELS data from Refs. 4 and 12.)

spond to a transition to the lowest unfilled MO. The present MO transition assignments follow those of Glen and Dodd[15] and also of Fischer,[42,43] who was the first to apply MO theory simultaneoulsy to the different-symmetry core edges. The parenthetic letters refer to the NES peaks as they are labeled in Figs. 2–10 (metal K edges) and Fig. 1 of Ref. 12 (oxygen K edges). WL denotes the metal L_3 white line; the OK peak labels are reproduced in Figs. 16–20. From the table and figures, we see that the quality of agreement between the NES of the three edges varies; each oxide is next considered in turn.

The most spectacular verification of the MO picture is shown in Fig. 16 for rutile TiO_2, where the spacings of the first two strong peaks in all three edges appear to be identical. (Actually, this spacing is wider in the Ti K edge; see Table III.) This observation supports the interpretation that the final states in all three transitions are in fact the same, namely, the $2t_{2g}$ and $3e_g$ antibonding orbitals. Since these two orbitals are combinations of the Ti $3d$ orbitals and O $2p$ orbitals probed by the Ti L_{23} and OK edges, respectively, we expect the strong transition strengths observed, while the relative weakness of the peaks in the Ti K edge is explained by the absence of p character in these molecular orbitals near the metal atom.

In Fig. 16 the Ti L_3 edge fine structure is ob-

TABLE III. Attempted determination of MO-energy-level spacings from the oxide core near-edge fine structures. The peak energies are measured relative to the first MO transition peak, through which the leftmost dotted line is drawn in Figs. 16–20. Results by other investigators (Refs. 16, 42, and 43) are also listed. The labels on the metal–K-edge peaks are from Figs. 2–10. WL denotes the metal L_3 white line.

Material	Edge	Reference	Exciton	$2t_{2g}$	$3e_g$	$3a_{1g}$	$4t_{1u}$
TiO_2 (rutile)	Ti L_3	Present study		0 (WL)	2.5		
	Ti K	Present study	−3.1 (A_1)	0 (A_2)	3.0 (A_3)	8.6 (B)	15.6 (C_1)
	O K	Present study		0 (b)	2.5 (b')	8.5 (c)	12.5 (d)
	Ti L_3	Fischer (Ref. 42)	−3.5 (f)	0 (b)	2.1 (c)		
	Ti K	Fischer (Ref. 42)		0 (b)	2.1 (c)	8.4	15.8
	O K	Fischer (Ref. 42)	−2.5 (f)	0 (b)	2.1 (c)		
	Ti K	Tsutsumi *et al.* (Ref. 16)		0	3.0	8.8	[13.3, 15.5]
TiO_2 (anatase)	Ti K	Present Study	−3.2 (A_1)	0 (A_2)	2.3 (A_3)	[7.5 (B_1), 11.1 (B_2)]	12.9 (C)
Cr_2O_3	Cr L_3	Present study		0 (WL)			
	Cr K	Present study		0 (A_1)	3.4 (A_2)	10.9 (B)	17.7 (C_1)
	O K	Present study		0 (b)	2.0 (b')	[6.5 (c), 11.0 (d)]	
	Cr L_3	Fischer (Ref. 43)	−3.1 (f)	0 (b)	2.6 (c)		
	Cr K	Fischer (Ref. 43)		0 (b)	2.6 (c)	9.0 (d)	15.0 (e)
	O K	Fischer (Ref. 43)	−1.8 (f)	0 (b)	2.6 (c)		
FeO	Fe L_3	Present study			0 (WL)	6.7	
	Fe K	Present study			0 (A)	12.0 (B)	18.4 (C)
	O K	Present study			0 (b)	6.0 (c)	9.0 (d)
Fe_2O_3	Fe K	Present study	−1.6 (A_1)		[0 (A_2), 2.0 (A_3)]	9.0 (B)	15.4 (C_1)
NiO	Ni L_3	Present study			0 (WL)	6.6	12.7
	Ni K	Present study			0 (A)	[3.5 (B_1), 8.6 (B_2)]	12.2 (B_3)
	0 K	Present study			0 (b)	[5.0 (c), 8.0 (d)]	14.5 (e)
CuO	Cu L_3	Present study			0 (WL)	7.6	13.2
	Cu K	Present study			0 (A)	8.3 (B_1)	[15.0 (B_2), 19.9 (C)]
	O K	Present study			0 (b)	[5.0 (c), 9.0 (d)]	14.0 (e)

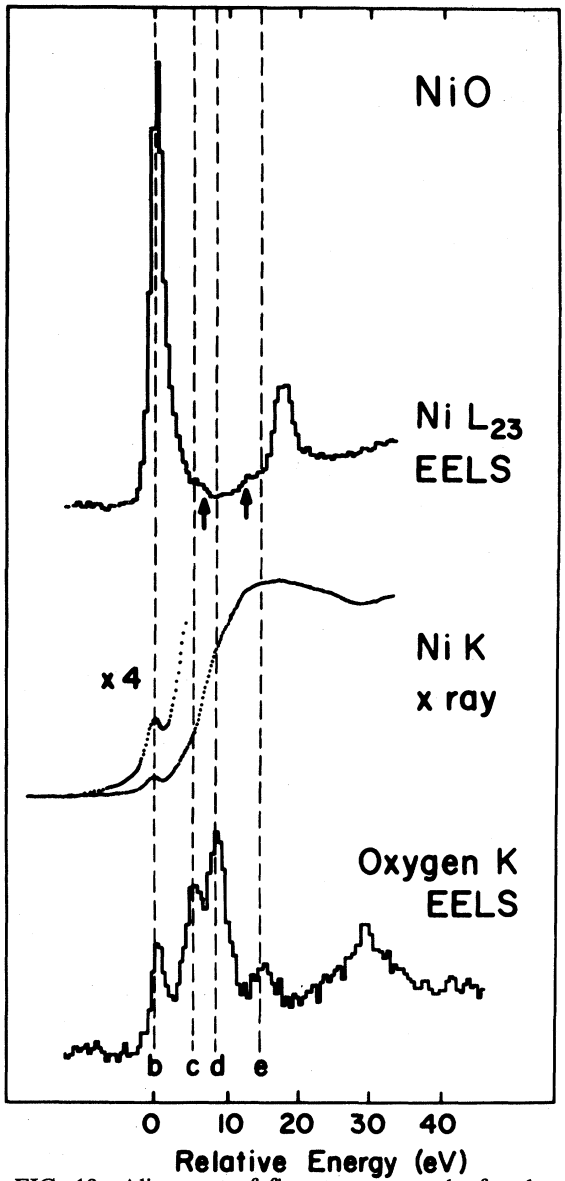

FIG. 19. Alignment of fine-structure peaks for three core edges in NiO. (EELS data from Refs. 4 and 12.)

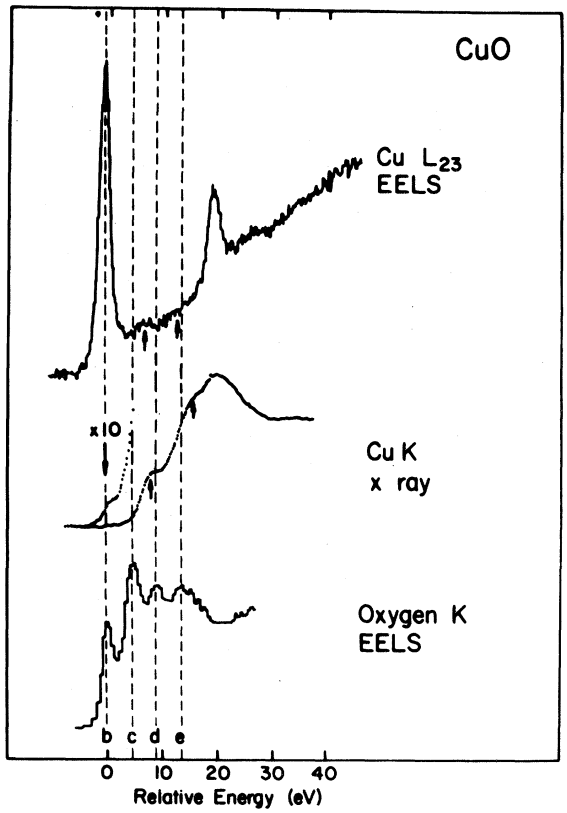

FIG. 20. Alignment of fine-structure peaks for three core edges in CuO. (EELS data from Refs. 4 and 12.)

scured from 6 eV above onset by the Ti L_2 edge, which also displays the $2t_{2g}$-$3e_g$ final-state splitting. The $3a_{1g}$ transition (peak c in the O K spectrum) matches well between the Ti K and O K spectra, while the agreement at higher energies degrades. Finally we note the presence of a weak feature on the Ti K edge, marked by an arrow below the $2t_{2g}$ transition peak. This feature has no MO interpretation, and so is labeled an exciton in Table III. A similar peak (A_1) also occurs in the anatase-phase spectrum; see Fig. 2.

Results by previous investigators[16,42] for rutile TiO_2 are also listed in Table III. The MO energy-level splittings are in fair agreement with ours. Note that Fischer[42] claims that all three edges display identical $2t_{2g}$-$3e_g$ splittings, although a close look at his data indicates otherwise. More importantly, Fischer's Ti L_3 and O K spectra both show a weak peak below the onset of the MO transitions, corresponding to the A_1 peak seen in the Ti K edge (in Figs. 2 and 16) and labeled as a core exciton. From Table III, we see that the binding energy of the core exciton below the conduction band (which here is defined as the onset of MO transitions) differs for all three core edges, and is largest for the Ti-atom excitations. This is in keeping with an excitonic assignment, since bonding charge transfer from Ti to O reduces valence-electron screening and thereby strengthens the electron-hole interaction around the Ti atom relative to the O atom.

In a recent paper,[12] we compared our experimentally derived MO energy-level splittings for rutile TiO_2 to peaks in the conduction-band DOS as calculated by Wilker and Hoffmann using extended Hückel tight-binding theory. This comparison is reproduced in Fig. 16, where the calculated DOS is shown in the top curve. (In our previous study,[12] we used Ti K-edge data by Tsutsumi *et al.*,[16] which did not show the weak peak at onset, marked by an arrow in Fig. 16.) As expected, the calculation pro-

duces a band-broadened version of the MO picture. Hence the calculated DOS does not predict the weak A_1 peak at onset in the Ti K edge (Fig. 2, Table III), indicating that this feature is not due to a one-electron transition. Since then, as an additional check, Wilker and Hoffmann have also computed the band structure and DOS for anatase-phase TiO_2.[44] Their total and Ti projected DOS for both phases are compared in Fig. 21, and these are quite similar. Neither phase shows a trace of a third distinct peak in the unoccupied portion of the DOS (unshaded areas) which might give rise to the third (A_1) peak observed in the core-edge spectra of both. We do note that the two peaks in the unfilled DOS centered at about 2.5 and 7 eV in the rutile phase are more widely spaced than in the anatase phase (about 2.7 and 6.5 eV), and this agrees with the $2t_{2g}$-$3e_g$ fine-structure splitting hierarchy measured in the respective Ti K edges (Table III). We also note that the peaks in the DOS for each phase are at identical energies in both the Ti and O projections. This corroborates our assertion that, within the one-electron transition model, the NES for excitations centered about different atoms in the same solid should be correlated.

Balzarotti *et al.*[45] have made a similar comparison of their measured Ti K edge in $SrTiO_3$ with an augmented-plane-wave band-structure calculation by Mattheiss.[46] The Ti atom is also octahedrally coordinated in this compound, and their Ti K edge shows three weak peaks at onset similar to the A_1, A_2, and A_3 peaks we observe in rutile- and anatase-phase TiO_2 (Fig. 2). However, in $SrTiO_3$, the middle spectral peak is very sharp while the third is quite broad, and this agrees with Mattheiss's calculated DOS where the lower-lying $2t_{2g}$-like band is much more sharply peaked than the diffuse higher-lying $3e_g$-like band. The calculated DOS again fails to exhibit any structure which could be connected to the initial weak spectral peak, corroborating the assignment of this feature in both TiO_2 and $SrTiO_3$ to a core exciton residing within the forbidden band gap.

Our three aligned edges for Cr_2O_3 are shown in Fig. 17. Once again, the $2t_{2g}$-$3e_g$ peak splitting is largest in the Cr K edge. The small Cr K peak marked by an arrow is 3.4 eV above the initial $2t_{2g}$ peak while the O K shoulder b' is only 2.0 eV above the main $2t_{2g}$ peak b (Table III). We fail to resolve any splitting in the Cr L_3 edge; fine structure past 9 eV above threshold is obscured by L_2 edge onset. Although the shoulder c in the O K edge has no analog in the Cr K edge, the peak d, assigned to the $3a_{1g}$ transition, matches well to the main Cr K shoulder B. There is no agreement at higher energies.

For Cr_2O_3 Fischer[43] again claims (see Table III) that all three edges display the same splitting energy, although a close look at his data again shows that the Cr K-edge peaks are more widely spaced. His reported $2t_{2g}$-$3e_g$ splitting of 2.6 eV falls between our Cr K and O K edge values, and probably represents a compromise. He also reports the weak pre-edge structure (f) in the Cr L_3 and O K edges and assigns it to a core exciton. As for TiO_2, the exciton binding energy is larger in the metal spectra (3.1 eV) than for oxygen (1.8 eV). We do not observe any such excitonic peak in our high-resolution, low-noise Cr—K-edge data.

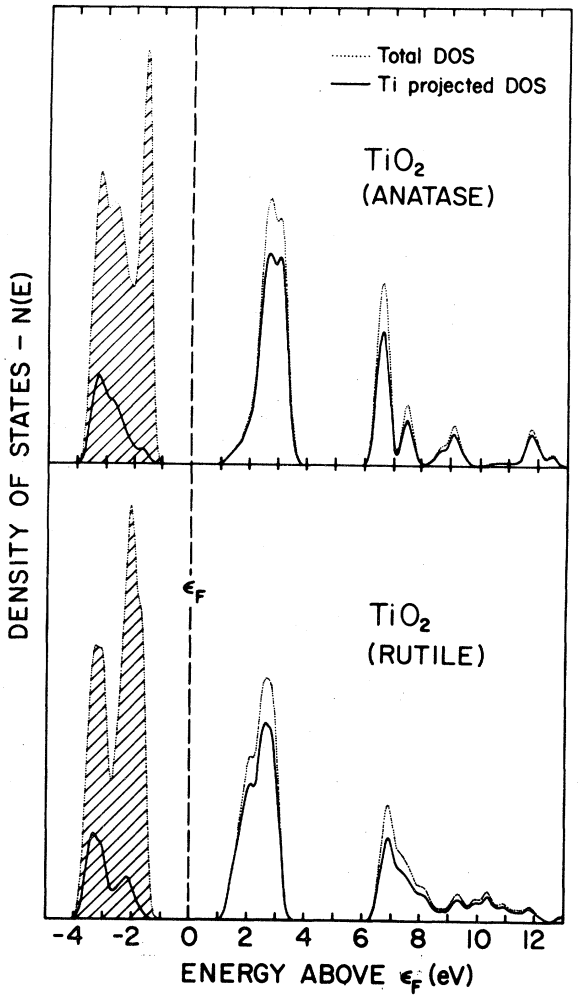

FIG. 21. Total and Ti projected DOS for rutile and anatase forms of TiO_2 as calculated by Wilker and Hoffmann (Ref. 44). Shaded regions denote occupied levels.

Figure 18 shows the edges for FeO, in which the $2t_{2g}$-$3e_g$ splitting is no longer discerned because the $2t_{2g}$ level is filled. The match between higher-lying MO transition peaks was not impressive for TiO_2 or Cr_2O_3, and the same applies for FeO. In particular, the Fe K edge has no feature corresponding to the shoulder c on the O K edge, although the dotted line

drawn through c is not far off the center of the weak bump marked by an arrow in the Fe L_3 edge. For the L_3 spectra in the metals, this bump has been identified as a transition to a $4p$ band centered on an adjacent metal atom but having some $3d$ character at the excited atom.[4,7] Ignoring relaxation-energy shifts, this interpretation cannot hold for the oxides, since a transition to a peak in the $4p$ DOS should also appear in the Fe K edge and there is no such matching feature.

The three edges in NiO are shown in Fig. 19 in which the lowest unfilled state is the $3e_g$ MO. The match between the different NES's is again unconvincing. The dotted lines drawn through peaks c and d in the O K edge are clearly at lower energies than the two small bumps marked by arrows in the Ni L_3 edge. As seen in Table III, these bumps are in fair agreement with the B_1 and B_2 maxima (Fig. 5) in the Ni K edge. This might be expected, since the core hole for these two edges is centered on the same atom creating similar excitonic effects.

Our present lack of agreement between the NES of the three core edges in NiO is consistent with our earlier comparison[12] to calculations by Kunz. There we found that the oxygen K NES in NiO bore no relation to the calculated one-electron transition probability. Rather, the first few peaks were identified by an additional calculation as core excitons, and hence no NES correlation would be expected.

Finally, Fig. 20 shows the CuO edges. Once again, the O K peak c has no analog in the other two spectra. Peak d has a reasonable match to the B_1 step marked by an arrow in the Cu K edge, but cleanly misses the two secondary bumps also marked by arrows in the Cu L_3 edge. As for NiO, the agreement between the two Cu core edges is better.

In summary, the attempted alignment of the three core edges near threshold has met with limited success. A good match was found in rutile-phase TiO_2 *above* the one-electron transition threshold for the relative $2t_{2g}$, $3e_g$, and $3a_{1g}$ peak separations. The agreement for Cr_2O_3 was less obvious, although all three edges still exhibited the $2t_{2g}$-$3e_g$ splitting in either our or Fischer's[43] data. In FeO, NiO, and CuO, where the $2t_{2g}$ level is filled, no such initial peak doublet was expected or observed. Agreement between the higher-energy peaks was not convincing for any of the sets of spectra, although a slightly better match was evinced between the metal L_3 and K edges, i.e., for excitations (and therefore core holes) centered about the same atom. However, the general failure of the spectra to match up signals the inadequacy of the one-electron transition MO picture and indicates that core-hole and other electron interactions cannot be neglected. (Speculations on the origin of the importance of core excitons in NiO versus unimportance in TiO_2 have been offered previously.[12]) We reached a similar conclusion in Sec. V, where we found that recent calculations for the metal K NES in compounds include the relaxed core hole and ascribe otherwise unexplained edge features to many-electron shakedown effects or to continuum resonances. However, these calculations, which partly corroborated the MO picture, were never extended to the O K or metal L_3 NES. In light of the present three-edge comparisons it seems that even more drastic many-body alterations of the NES such as the electron-hole interactions described above are taking place.

VII. SUMMARY AND CONCLUSIONS

We have presented the K edges of selected $3d$ transition metals and oxides as measured by x-ray absorption at the Cornell High Energy Synchrotron Source. Oxide-metal chemical shifts are all positive. Such behavior was expected on the basis of core-level shifts neglecting final-state effects, but was not observed in our previous studies of the metal M_1 or L_3 edges. The multipeaked fine structure observed in the near-edge region is consistent with previous investigations. For the metals, we find an excellent match between our data and one-electron calculations for these edges. Minor differences near threshold may be due to many-body alterations of the line shape, while slight systematic differences between experimental and theoretical energy scales may be due to the neglect by theory of the core hole. Calculations for the oxide NES are less developed. Several authors have used symmetry-based molecular-orbital arguments to assign the various NES peaks to one-electron transitions to unoccupied orbitals. However, these assignments are in doubt, since the poorly screened core hole is expected to give rise to gross many-body alterations of the spectra. Recent calculations indicate that while some of the near-edge peaks are indeed attributable to one-electron transitions whose energies are modified by the presence of the core hole, other features have no such simple origin.

Next, we continue our interpretation of the NES in the oxides by considering the metal L_{23}, metal K, and oxygen K edges altogether. Using MO theory, we attempt to correlate the NES of these three edges for each oxide. In particular, comparisons are made between the fine-structure peak spacings in an attempt to verify the consistency of the inferred MO energy-level spacings.

For TiO_2 (and perhaps Cr_2O_3), the three symmetry edges display structures consistent with each other and with MO theory. However, the weak peak

evinced in our Ti K edges in both rutile and anatase forms of TiO_2 is unexplained by MO theory or band-structure calculations, and must be attributed to a core-exciton final state residing in the valence- to conduction-band gap. We conclude that the core edges in TiO_2 are fairly well described *above* the one-electron transition threshold by the DOS of the unperturbed solid. On the other hand, for FeO, NiO, and CuO, the NES of the three core edges fail to match up, repudiating the one-electron interpretation of the data. Rather, we are forced to conclude that the core excitation spectra in these oxides must be dominated near threshold by core excitons and not by transitions to peaks in the unfilled DOS of the initial, unperturbed solid. The strength of core-hole interaction is *not* expected to be the same for excitations of the metal versus oxygen-atom core excitons (see, e.g., Ref. 4). Hence the presence of core excitons explains the observed lack of correlation between peaks in the near-edge structure for different chemical species in the same solid.

ACKNOWLEDGMENTS

The author would like to thank Professor J. Silcox, Professor J. W. Wilkins, Professor E. A. Stern, and Professor K. Tsutsumi, and Dr. J. E. Müller, Dr. D. M. Mills, Dr. C. N. Wilker, and Dr. R. D. Leapman for helpful discussions and communications. Also special thanks are due to Dr. D. M. Mills, M. T. King, and the rest of the CHESS staff for their kind assistance. Support from the National Science Foundation through the Cornell Materials Science Center Grant No. NSF DMR-79-24008 is gratefully acknowledged.

---

*Present address: Xerox Webster Research Center, Bldg. 114, 800 Phillips Road, Webster, NY 14580.

[1]This article is drawn from L. A. Grunes, Ph.D. thesis, Cornell University, 1982 (unpublished).

[2]A. Kotani and Y. Toyozawa, in *Synchrotron Radiation,* edited by C. Kunz (Springer, New York, 1979).

[3]U. Fano and J. W. Cooper, Rev. Mod. Phys. 40, 441 (1968).

[4]R. D. Leapman and L. A. Grunes, Phys. Rev. Lett. 45, 397 (1980); R. D. Leapman, L. A. Grunes, and P. L. Fejes, Phys. Rev. B 26, 614 (1982).

[5]L. V. Azaroff and D. M. Pease, in *X-ray Spectroscopy,* edited by L. V. Azaroff (McGraw-Hill, New York, 1974).

[6]J. E. Müller, Ph.D. thesis, Cornell University, 1980 (unpublished).

[7]J. E. Müller, O. Jepsen, and J. W. Wilkins, Solid State Commun. 42, 365 (1982), and private communication.

[8]D. J. Nagel, D. A. Papaconstantopoulos, J. W. McCaffrey, and J. W. Criss, *Proceedings of the International Symposium on X-ray Spectra and Electronic Structure of Matter,* edited by A. Faessler and G. Wiech (Academic, New York, 1973), p. 51.

[9]L. A. Grunes and R. D. Leapman, Phys. Rev. B 22, 3778 (1980).

[10]H. P. Hjalmarson, H. Buttner, and J. D. Dow, Phys. Rev. B 24, 6010 (1981).

[11]E. A. Stern and J. J. Rehr (unpublished), and private communication.

[12]L. A. Grunes, R. D. Leapman, C. N. Wilker, R. Hoffmann, and A. B. Kunz, Phys. Rev. B 25, 7157 (1982).

[13]D. M. Mills and M. T. King (private communication).

[14]W. W. Beeman and H. Friedman, Phys. Rev. 56, 392 (1939).

[15]G. L. Glen and C. G. Dodd, J. Appl. Phys. 39, 5372 (1968).

[16]K. Tsutsumi, O. Aita, and K. Ichikawa, Phys. Rev. B 15, 4638 (1977), and private communication.

[17]K. Ichikawa, O. Aita, H. Nakamori, M. Kamada, and K. Tsutsumi, Jpn. J. Appl. Phys. 17, Suppl. 17-2, 157 (1978).

[18]C. Sugiura and S. Nakai, Jpn. J. Appl. Phys. 17, Suppl. 17-2, 190 (1978).

[19]M. Belli, A. Scafati, A. Bianconi, S. Mobilio, L. Palladino, A. Reale, and E. Burattini, Solid State Commun. 35, 355 (1980).

[20]D. R. Sandstrom, R. H. Filby, F. W. Lytle, and R. B. Greegor, Fuel 61, 195 (1982).

[21]D. A. Papaconstantopoulos, D. J. Nagel, and C. Jones-Bjorkland, Int. J. Quantum Chem. Symp. 12, 497 (1978).

[22]S. Wakoh and Y. Kubo, Jpn. J. Appl. Phys. 17, Suppl. 17-2, 193 (1978).

[23]F. Szmulowicz and D. M. Pease, Phys. Rev. B 17, 3341 (1978).

[24]J. E. Müller, O. Jepsen, and J. W. Wilkins, Solid State Commun. 42, 365 (1982); see also Refs. 4 and 6.

[25]R. A. Bair and W. A. Goddard, Phys. Rev. B 22, 2767 (1980).

[26]F. W. Kutzler, C. R. Natoli, D. K. Misemer, S. Doniach, and K. O. Hodgson, J. Chem. Phys. 73, 3274 (1980).

[27]J. A. Bearden and A. F. Burr, Rev. Mod. Phys. 39, 125 (1967).

[28]See, e.g., Ref. 23 and D. M. Pease, Appl. Spectrosc. 30, 405 (1976).

[29]G. Materlik, J. E. Müller, and J. W. Wilkins, Phys. Rev. Lett. 50, 267 (1983); J. W. Wilkins (private communication).

[30](a) J. F. Herbst and J. W. Wilkins, Phys. Rev. B 20,

2999 (1979); J. W. Wilkins (private communication). (b) C. Noguera, D. Spanjaard, and J. Friedal, J. Phys. F 6, 1189 (1979); C. Noguera and D. Spanjaard, *ibid.* 11, 1133 (1981).

[31]P. H. Citrin, G. K. Wertheim, and M. Schlüter, Phys. Rev. B 20, 3067 (1979).

[32]J. Müller and W. Schaich, Bull. Am. Phys. Soc. 26, 320 (1981), abstract EP6.

[33]See, e.g., P. J. Durrant and B. Durrant, *Introduction to Advanced Inorganic Chemisty,* 2nd ed. (Longman Group, London, 1970), p. 976.

[34]R. G. Shulman, Y. Yafet, P. Eisenberger, and W. E. Blumberg, Proc. Natl. Acad. Sci. USA 73, 1384 (1976).

[35]A. Viste and H. B. Gray, Inorg. Chem. 3, 1113 (1964).

[36]J. A. Tossell, D. J. Vaugham, and K. H. Johnson, Am. Mineral. 59, 319 (1974).

[37]L. Grunes and R. D. Leapman, in Proceedings of the Cornell Analytical Electron Microscopy Workshop, 1978, Cornell Materials Science Center Report No. 3082 (unpublished); p. 118.

[38]S. K. Pantelides, Phys. Rev. B 11, 2391 (1975).

[39]E. J. Mele and J. J. Ritsko, Phys. Rev. Lett. 43, 68 (1979).

[40]F. C. Brown, in *Solid State Physics,* edited by H. Ehrenreich, F. Seitz, and D. Turnbull (Academic, New York, 1974), Vol. 29, p. 1, and references therein.

[41]E. E. Koch, C. Kunz, and B. Sonntag, Phys. Rep. 29C, 153 (1977), and references therein.

[42]D. W. Fischer, Phys. Rev. B 5, 4219 (1972).

[43]D. W. Fischer, J. Phys. Chem. Solids 32, 2455 (1971).

[44]C. N. Wilker and R. Hoffmann (private communication).

[45]A. Balzarotti, F. Comin, L. Incoccia, M. Piacentini, S. Mobilio, and A. Savoia, Solid State Commun. 35, 145 (1980).

[46]L. F. Mattheiss, Phys. Rev. B 6, 4718 (1972).